Enhancing fracture permeability due to in-situ mineral carbonation: an experimental investigation into reaction-driven cracking in ultramafic rocks

Clay Wood[1,2], Nicola Tisato[1], Nicolas Esinoza[2], Estibalitz Ukar[3]

[1] Dept. of Earth and Planetary Sciences, Univeristy of Texas at Austin, [2] Hildebrand Dept. of Petroleum and Geosystems Engr., University of Texas at Austin, [3] Bureau of Economic Geology, University of Texas at Austin

Ultramafic formations are favorable to CO_2 sequestration

Global pressures to sequester CO2 and reduce emissions:

- Economic incentives for novel methods to reduce critical mineral extraction energy &and increase yield due to shift from hydrocarbons
- Permanent CO2 sequestration presents many challenges (e.g. time scale, monitoring)

Ultramafic formations are compelling sites:

- Mineral constituents (olivine, brucite) are energetically favorable for reaction with CO2 -- permanent mineral trapping
- Reaction kinetics may increase porosity & fracture networks and decrease strength
- Possibility of extracting reaction products
- Previous carbon mineralization work is primarily ex-situ capture
- In-situ injection offers of orders of magnitude greater storage capacity.
- Reaction kinetics show increase in solid volume as much as 40% —> penetrative carbonate-mineral-filled fracture network — reaction-driven cracking

Questions driving this work:

How can we leverage chemo-poro-mechanical processes to sustain reaction at field conditions?

How does CO2 sequestration change the mechanical strength of the subsurface?

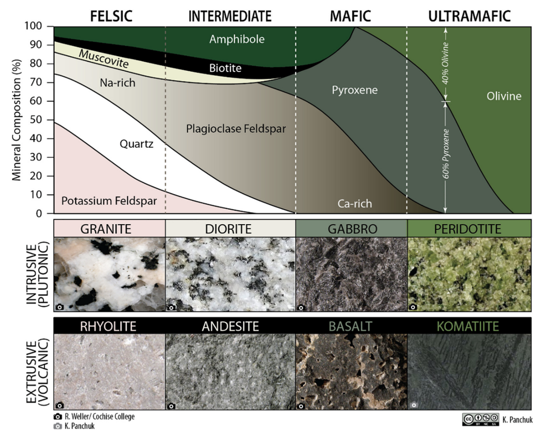

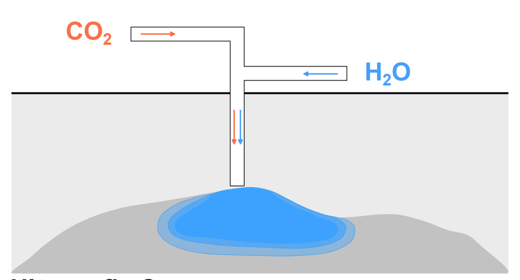

Ultramafic Core

Simulating field conditions and kinetics in the laboratory

We use laboratory experiments in order to investigate the complex interplay between the poromechanics and kinetics in the subsurface. One of the goals is to develop methods and techniques for enhancing pore and fracture network permeability to increase the CO storage potential of ultramafics. Here, we present a novel experimental apparatus that injects carbonated water into ultramafic samples, provided by Canada Nickel Company, for long durations -- several months. To the right is a fractured sample imaged with micro-CT.

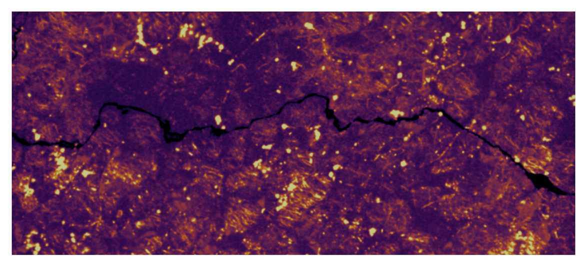

Ultramafic core characterization & sample preparation

Ultramific samples were cored to 25.4 mm diameter and 45 mm long from larger cores provided by Canada Nickel Company. During preparation, a tensile fracture formed along the length of the core. Both ends were flattened and to within < 0.25 mm. Then, the sample was placed between two endcaps (more details in next section).

Teflon tubing was placed around the core assembly then shrunk. Lacing wire on each endcap ensures a permanent sealing -- preventing pore fluidings from mixing with confining fluid. Finally, the sample configuration is attached to the top piece of the pressure vessel and sealed inside.

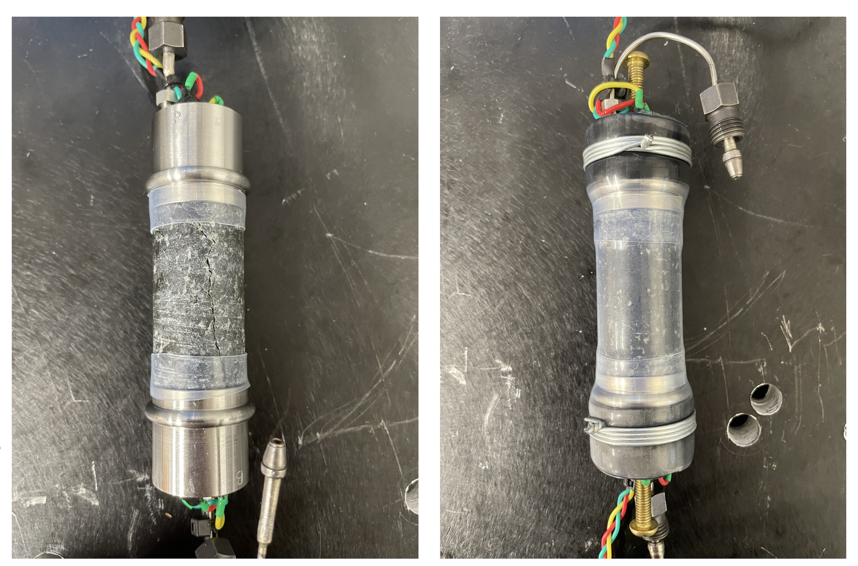

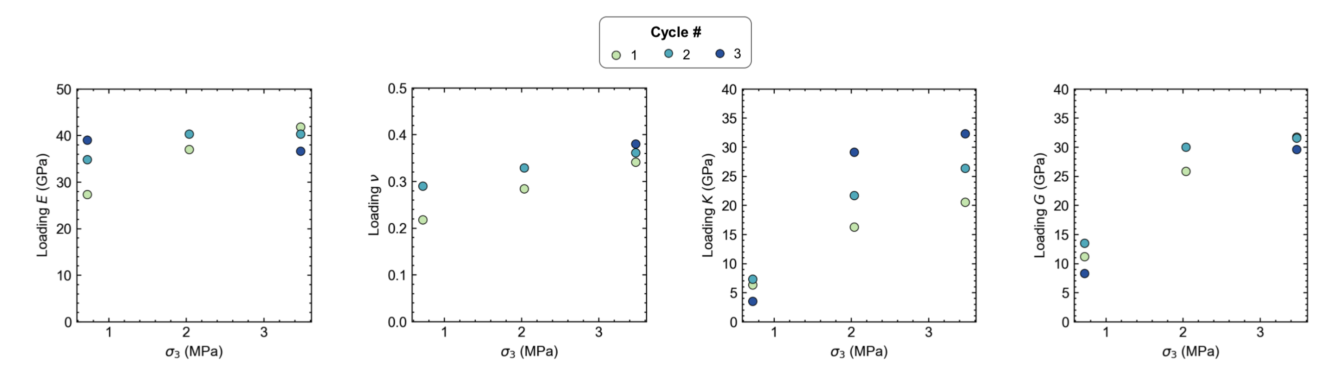

In addition to injection experiments, elastic properties were measured for samples provided by Canada Nickel Company. The figure above shows measurements of elastic moduli and Poisson ratio for a 25.4 mm diameter ultramafic samples. The samples were sealed and fixed inside of triaxial apparatus and underwent isotropic compression and deviotoric stress tests with loading/unloading cycles at different confining pressures, s3, before bringing to failure.

Experimental configuration

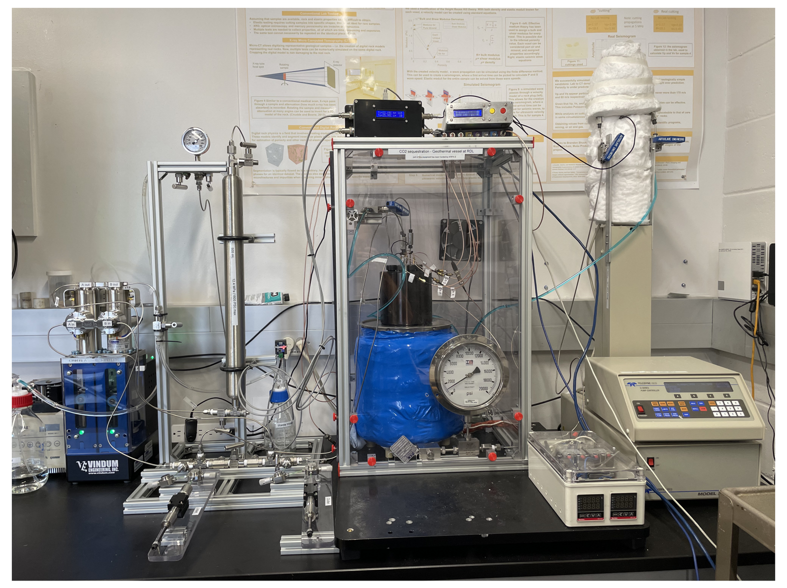

Overview photo of experimental apparatus developed for this project. There are 3 novel aspects about this custom-built apparatus: (1) a pressure vessel with temperature control up to 300 C, (2) continuous acquisition at 10 MHz of acoustic emisisons, and (3) long-term stability on order of months or longer.

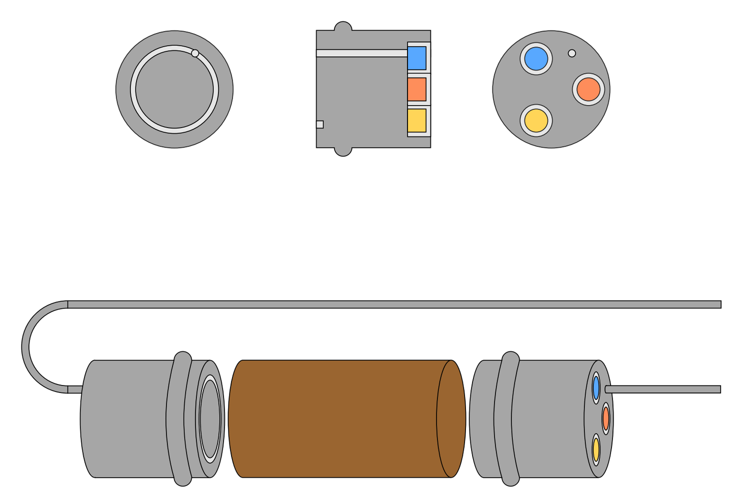

(a) Bottom face of end cap has a through-fluid port and circular groove to evenly distribute flow. **(b)** End cap side view, showing position of embedded piezoelectric transducers (PZTs), colored. **(c)** Orientation of PZTs shown in top view of end cap, allowing for P, S_1, S_2 transducers. **(d)** Schematic of position of end caps with fluid lines and sample.

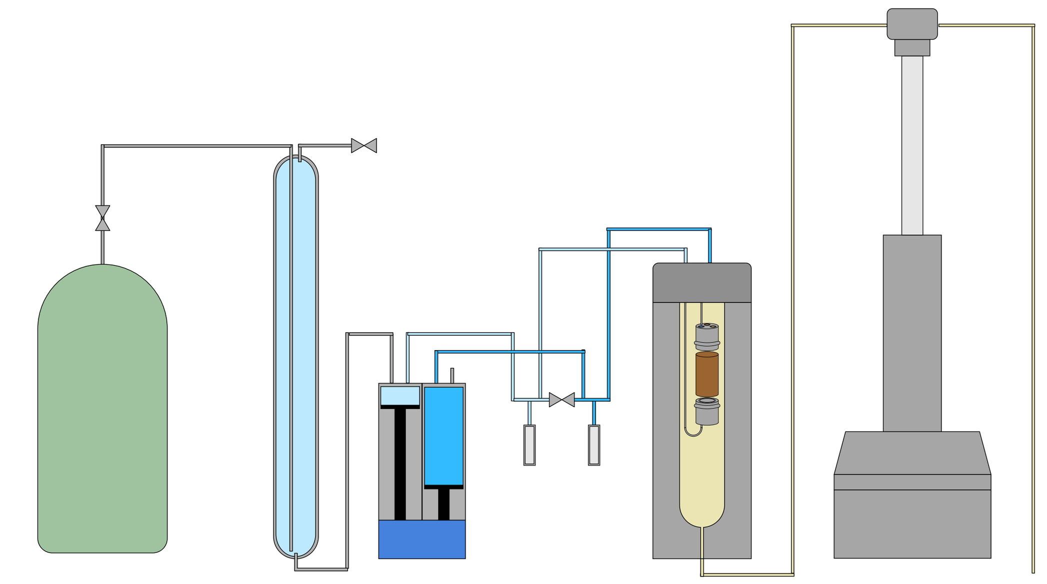

Schematic of injection apparatus. **(a)** CO_2 cylinder and mixing reservoir are used to carbonate water before injection. **(b)** Vindum pump with independently-controlled cylinders injects carbonated water into the sample. **(c)** Simplified fluid manifold with collection syringes that allow for sampling inlet/outlet fluids at pressure. **(d)** Sample prepared and then sealed inside of the pressure vessel and Isco pump maintains constant hydrostatic pressure -- simulating pressure of field site.

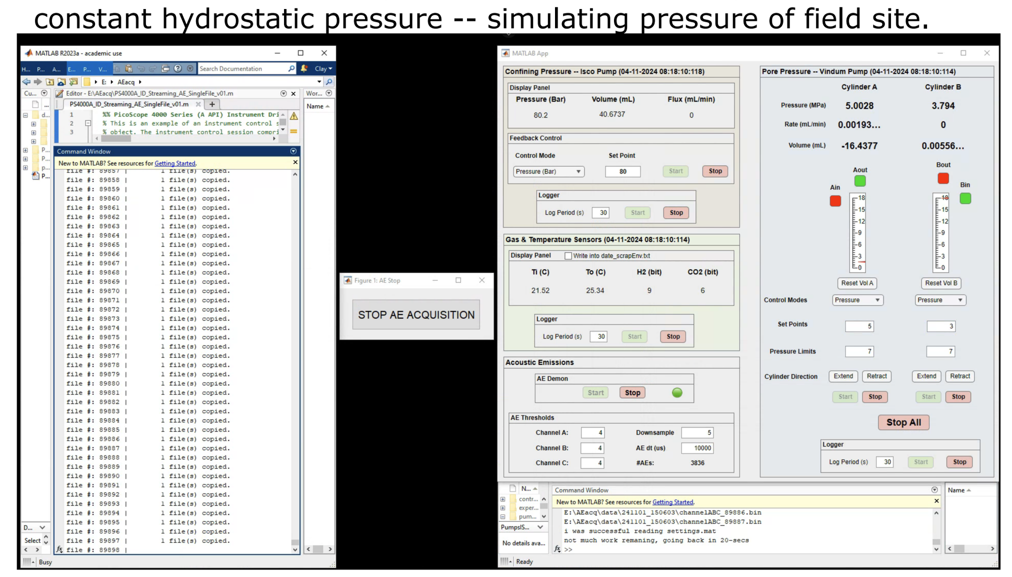

Software was developed in-house to control apparatus. (a) Continuous acquisition from Picoscope at 10 MHz to record acoustic emissions. (b) Panel to control and record from Isco pump for confining pressures. (c) Panel to record from temperature and environmental sensors. (d) Panel to begin background analysis for acoustic emissions. (e) Panel to control and record from Vindum pump for injection.

Long-term experiment shows trend in permeability enhancement

The first experiment, using a pre-fractured ultramafic sample, lasted for 70, demonstrating one of the main goals -- long-term stability and time-scales relevant to field injection studies.

Mechanical data from confining pressure pump. **(a)** Confining pressure Pc is maintained at a constant 10 MPa for the duration of the experiment . **(b)** Volume change of confining pump cylinder.

Flow data from injection pump. **(c)** The inlet pressure was kept constant at 2.3 MPa. **(d)** The outlet cylinder was maintained at a flow rate of ~ 0.01 mL/min ~= 1.67*10^-10 m^3/s. **(e)** Permeability during steady-state flow (Qin = Qout, within 1%) during the experiment.

Insets from experiment data overview. **(f)** and **(g)** show the relative change in confining cylinder volume and permeability, respectively as a function of log-time.

The main take-away is a systematic permeability enhancement of nearly 100x over 70 days. This is primarily attributed to dissolution-dominated kinetics, eroding the fracture aperture.

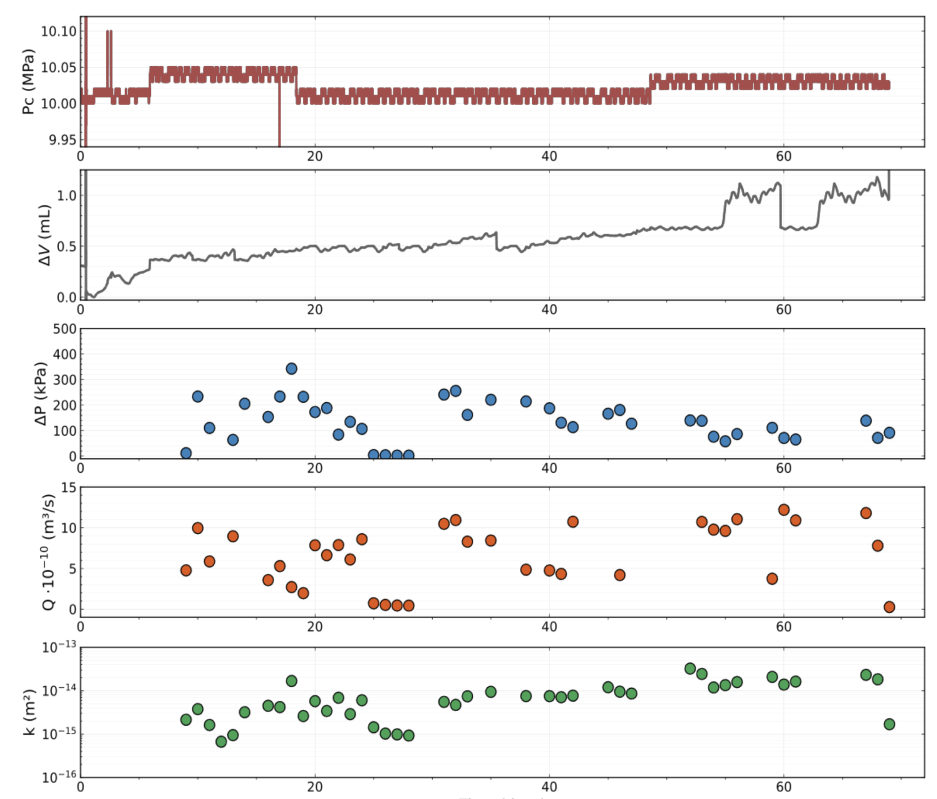

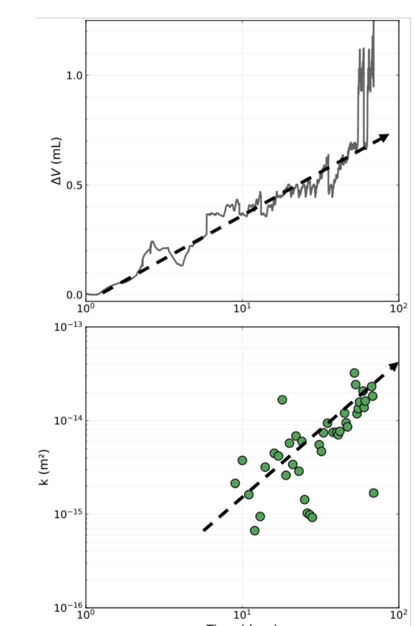

Carbon mineralization and fracture closure

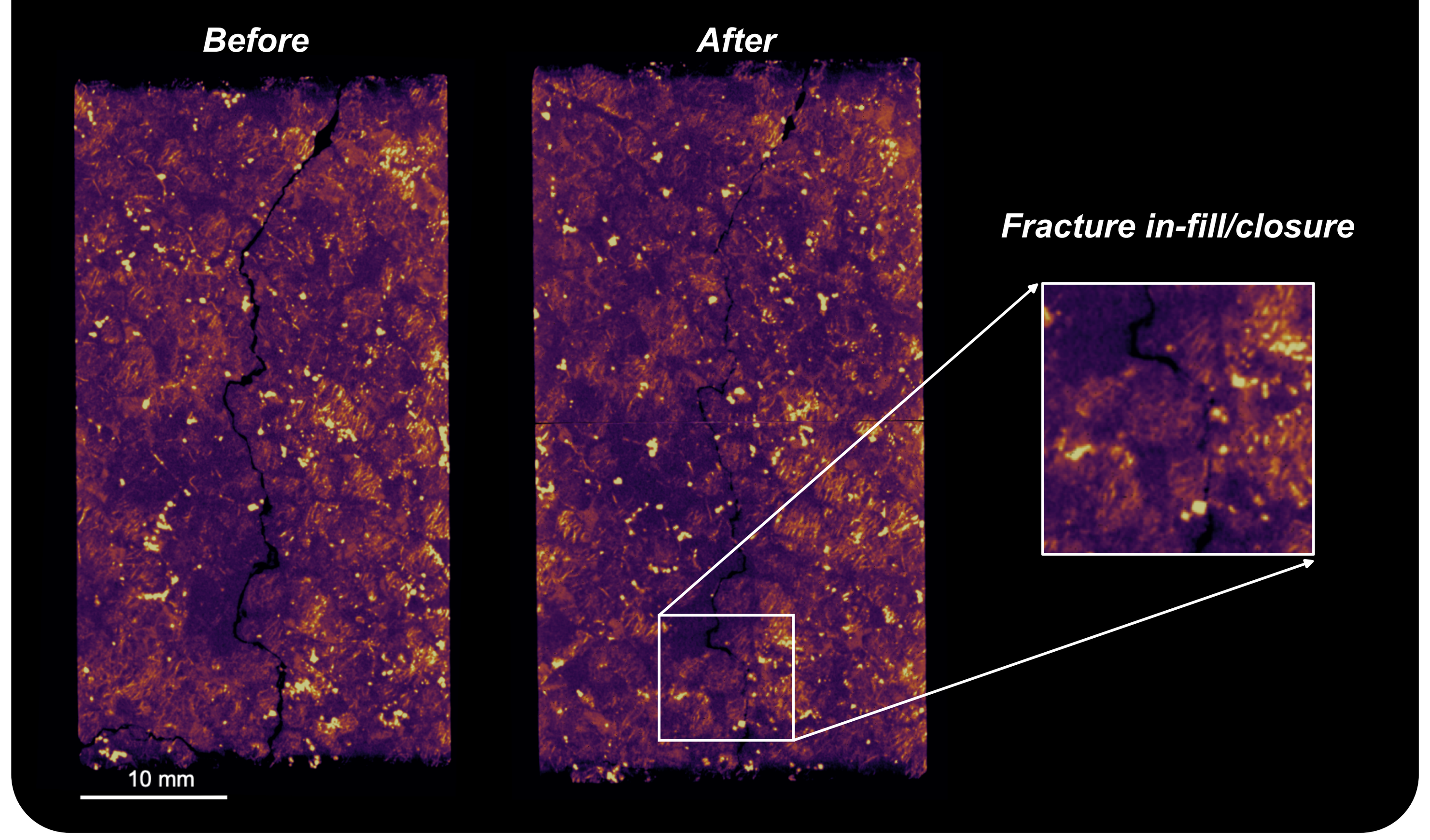

Figure above shows 2D slices from micro-CT volumes of the fractured sample before and after the 70 days long injection experiment. Darker colors correspond to minerals with lower density and brigher colors correspond to minerals with higher density. Though chemical analysis is on-going, the main observation is fracture in-fill from reaction along the fracture plane -- more prevalent at outlet side.

Acoustic emissions attributed to fracture deformation

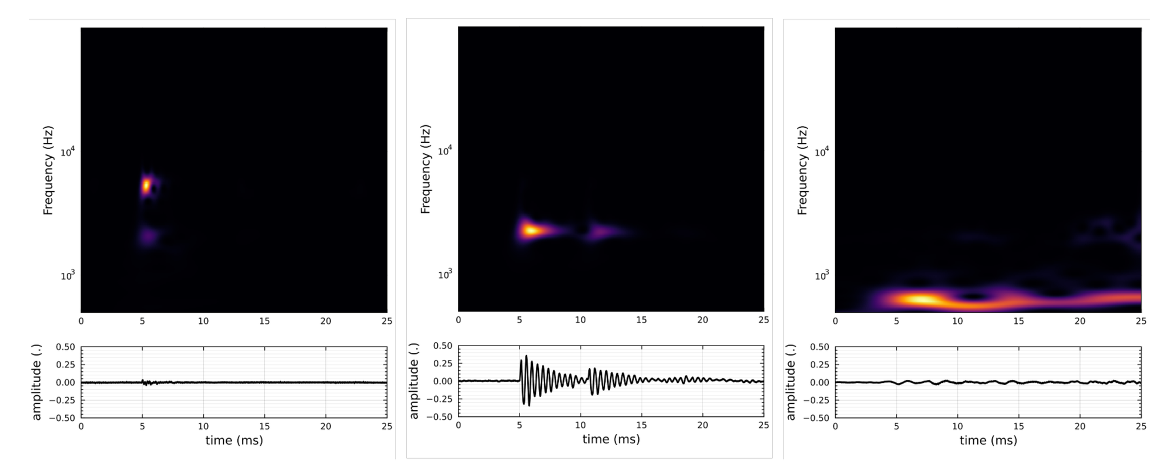

Gallery of acoustic emissions recorded from 2nd experiment where cylindrical ultramafic sample with brucite vein. Figure above illustrates the range of dominant frequencies and normalized amplitudes in acoustic emissions recorded during the experiment. Preliminary analysis indicates that these are primarliy attributed to vein/fracture deformation rather than reaction-driven cracking. Low frequency events could be linked to fluid-induced, but further analysis and testing is required.

Possible mechanisms to enhance precipitation

Equations describing dissolution of carbonated water and brucite (Mg(OH)$_2$) and concentration change for a given chemical species.

$$\mathrm{CO_2 + H_2O \rightleftharpoons H_2CO_3 \rightleftharpoons H^+ + HCO_3^- \rightleftharpoons 2H^+ + CO_3^{2-}}$$

$$\mathrm{Mg(OH)_2 = Mg^{2+} + 2OH^-}$$

$$R_i = K_i \cdot A_{\mathrm{Mg(OH)_2}}$$

$$\frac{d[\mathrm{CO_2}]}{dt} = -\frac{R_{\mathrm{CO_2\ diss}}}{V_{\mathrm{H_2O}}}$$

$$\frac{d[\mathrm{Mg^{2+}}]}{dt} = \frac{R_{\mathrm{Mg(OH)_2\ diss}}}{V_{\mathrm{H_2O}}}$$

$$\frac{\partial c}{\partial t} = R - \nabla \cdot \mathbf{j}$$

$$\mathbf{j}_{\mathbf{diff}} = -D\nabla c = 0$$

$$\mathbf{j}_{\mathbf{adv}} = \mathbf{v}c$$

$$\frac{\partial c}{\partial t} = R - \nabla \cdot \mathbf{j}_{\mathbf{adv}} = R_i - \frac{Q}{A\ l_{frac}} c_i$$

Figure to the right shows numerical results of concentration of Mg2+ as a function of time for varying flow rates and fracture areas. The real fracture cross-sectional area is ~ 2.5 * 10^{-6} m^2. The flow rates are as follows: **(a)** 0 m^3/s, **(b)** 10^{-12} m^3/s, **(c)** 10^{-10} m^3/s, and **(d)** 10^{-8} m^3/s. This preliminary numerical estimation highlights the importance of ***fracture area and flow rate***:

- large brucite surface area greatly enhances precipitation
- flow rates faster than precipition inhibit preciptation

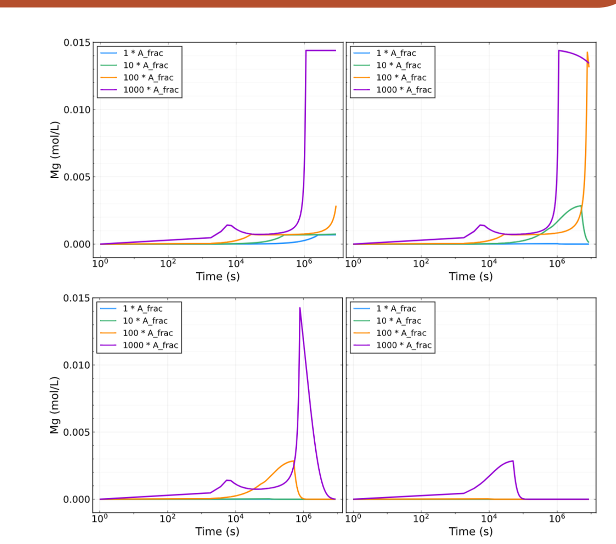

This work is supported by ARPA-E XXXX to EU